The Astrophysical Journal Letters, 950:L19 (10pp), 2023 June 20 https://doi.org/10.3847/2041-8213/acd6f6

© 2023. The Author(s). Published by the American Astronomical Society.

OPEN ACCESS

Astrometric Accelerations as Dynamical Beacons: A Giant Planet Imaged inside the Debris Disk of the Young Star AF Lep

Kyle Franson[1,11], Brendan P. Bowler[1], Yifan Zhou[1,12], Tim D. Pearce[2], Daniella C. Bardalez Gagliuffi[3,4], Lauren I. Biddle[1], Timothy D. Brandt[5], Justin R. Crepp[6], Trent J. Dupuy[7], Jacqueline Faherty[4], Rebecca Jensen-Clem[8], Marvin Morgan[1], Aniket Sanghi[1], Christopher A. Theissen[9,13], Quang H. Tran[1], and Trevor N. Wolf[10]

[1] Department of Astronomy, The University of Texas at Austin, Austin, TX 78712, USA
[2] Astrophysikalisches Institut und Universitätssternwarte, Friedrich-Schiller-Universität Jena, Schillergäßchen 23, D-07745 Jena, Germany
[3] Department of Physics & Astronomy, Amherst College, 25 East Drive, Amherst, MA 01003, USA
[4] American Museum of Natural History, 200 Central Park West, New York, NY 10024, USA
[5] Department of Physics, University of California, Santa Barbara, Santa Barbara, CA 93106, USA
[6] Department of Physics, University of Notre Dame, 225 Nieuwland Science Hall, Notre Dame, IN 46556, USA
[7] Institute for Astronomy, University of Edinburgh, Royal Observatory, Blackford Hill, Edinburgh, EH9 3HJ, UK
[8] Astronomy & Astrophysics Department, University of California, Santa Cruz, CA 95064, USA
[9] Center for Astrophysics and Space Sciences, University of California, San Diego, 9500 Gilman Drive, La Jolla, CA 92093, USA
[10] Department of Aerospace Engineering and Engineering Mechanics, The University of Texas at Austin, Austin, TX 78712, USA

Received 2023 February 10; revised 2023 May 5; accepted 2023 May 19; published 2023 June 22

Abstract

We present the direct-imaging discovery of a giant planet orbiting the young star AF Lep, a 1.2 $M_\odot$ member of the 24 ± 3 Myr β Pic moving group. AF Lep was observed as part of our ongoing high-contrast imaging program targeting stars with astrometric accelerations between Hipparcos and Gaia that indicate the presence of substellar companions. Keck/NIRC2 observations in L' with the vector vortex coronagraph reveal a point source, AF Lep b, at $\approx$340 mas, which exhibits orbital motion at the 6σ level over the course of 13 months. A joint orbit fit yields precise constraints on the planet's dynamical mass of $3.2^{+0.7}_{-0.6}\,M_{\rm Jup}$, semimajor axis of $8.4^{+1.1}_{-1.3}$ au, and eccentricity of $0.24^{+0.27}_{-0.15}$. AF Lep hosts a debris disk located at $\sim$50 au, but it is unlikely to be sculpted by AF Lep b, implying there may be additional planets in the system at wider separations. The stellar inclination ($i_* = 54^{+11}_{-9}{}^\circ$) and orbital inclination ($i_o = 50^{+9}_{-12}{}^\circ$) are in good agreement, which is consistent with the system having spin–orbit alignment. AF Lep b is the lowest-mass imaged planet with a dynamical mass measurement and highlights the promise of using astrometric accelerations as a tool to find and characterize long-period planets.

Unified Astronomy Thesaurus concepts: Extrasolar gaseous giant planets (509); Astrometric exoplanet detection (2130); Direct imaging (387); Orbit determination (1175); Debris disks (363)

1. Introduction

A growing number of planets with masses spanning 1–13 $M_{\rm Jup}$ and separations from $\approx$5 to 100 au have been imaged over the past 15 yr (e.g., Marois et al. 2008, 2010; Lagrange et al. 2010; Rameau et al. 2013; Macintosh et al. 2015; Chauvin et al. 2017; Keppler et al. 2018). It remains unclear whether these long-period "super Jupiters" predominantly form through a bottom-up core accretion scenario (Pollack et al. 1996), possibly assisted by pebble accretion (Johansen & Lambrechts 2017); through a top-down gravitational instability route (Boss 1997); or even via dynamical capture in a dense cluster at an early age (Perets & Kouwenhoven 2012). Further complicating the picture, the star formation process is expected to produce objects with masses as low as the opacity limit of $\sim$3 $M_{\rm Jup}$ through cloud fragmentation (Bate 2009). Demographic studies are hinting that imaged wide-separation planets have a bottom-heavy mass distribution (Wagner et al. 2019), a semimajor axis distribution weighted toward smaller separations (Nielsen et al. 2019), an eccentricity distribution peaked at low values in contrast to higher-mass substellar companions (Bowler et al. 2020; Nagpal et al. 2023), and preferentially aligned stellar obliquities (Bowler et al. 2023). These results resemble the demographics of closer-in planets found with radial velocities (RVs; e.g., Fulton et al. 2021) although the significance of this similarity is limited by the small number of imaged planets.

An efficient strategy to identify long-period companions is to use the gravitational reflex motion they induce on their host stars. Beginning with the discovery of the brown dwarf companion HR 7672 B (Liu et al. 2002), RV trends have been repeatedly used to identify promising targets for follow-up high-contrast imaging (e.g., Crepp et al. 2014; Cheetham et al. 2018; Bowler et al. 2021). More recently, astrometric accelerations using proper motion differences between Hipparcos and Gaia have proven to be similarly advantageous as a strategy to efficiently search for and characterize substellar companions (e.g., De Rosa et al. 2019; Brandt et al. 2019; Franson et al. 2022; Hinkley et al. 2023; Currie et al. 2023).

The Astrometric Accelerations as Dynamical Beacons program is a high-contrast imaging survey targeting a dynamically informed sample of young accelerating stars

---

[11] NSF Graduate Research Fellow.
[12] 51 Pegasi b Fellow.
[13] NASA Sagan Fellow.

Original content from this work may be used under the terms of the Creative Commons Attribution 4.0 licence. Any further distribution of this work must maintain attribution to the author(s) and the title of the work, journal citation and DOI.

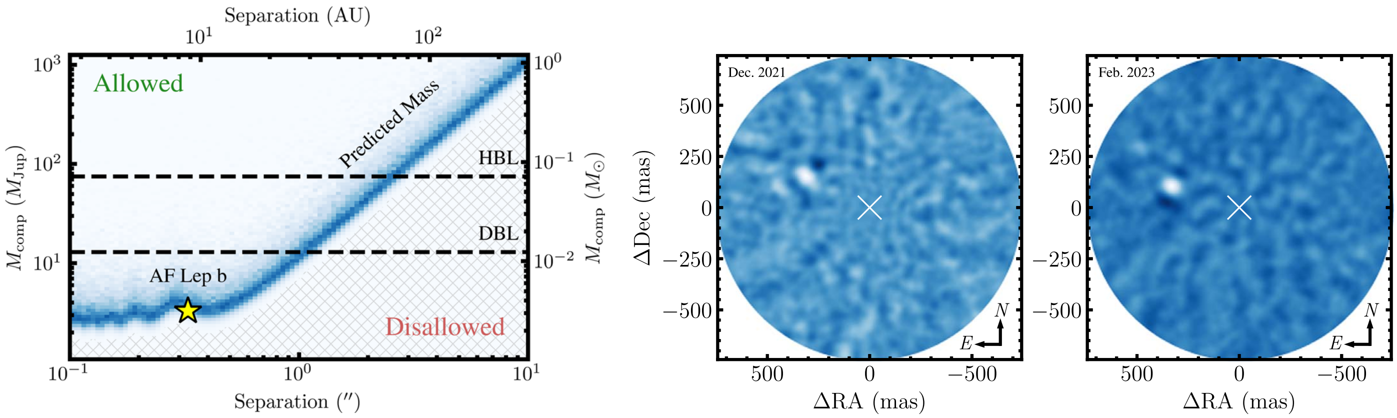

Figure 1. Left: predicted mass as a function of separation for AF Lep b from its HGCA astrometric acceleration. This plot is generated following Franson et al. (2023). The blue curve shows the masses and separations most consistent with the astrometric acceleration. Due to orbital phase, companions can occupy separations and masses above but not below the curve. The dynamical mass and semimajor axis of AF Lep b is denoted by the gold star. The planet is consistent with causing the acceleration. Right: Keck/NIRC2 Imaging L' imaging of AF Lep b in 2021 December (left) and 2023 February (right). Here, S/N plots are displayed to enhance true sources over residual speckles. Note that the two images do not share the same color map. We apply a Gaussian filter with a standard deviation of 1.5 pixels to average over pixel-to-pixel noise. AF Lep b is detected with a significance of 7.5σ in the 2021 December epoch and 13.0σ in the 2023 February epoch.

identified in the Hipparcos-Gaia Catalog of Accelerations (HGCA; Brandt 2021). Our targets are selected for youth, proximity, and from individual predictions of the companion mass and separation required to produce the observed proper motion difference between Hipparcos and Gaia EDR3. The first discovery from this program was the low-mass brown dwarf HIP 21152 B (Franson et al. 2023), a T-dwarf companion in the Hyades cluster.

Here we present the discovery of a giant planet orbiting the young star AF Lep[14] based on observations with the NIRC2 vector vortex coronagraph (VVC) at the Keck II telescope. In Section 2, we summarize the physical and astrometric properties of AF Lep. Our NIRC2 observations and analysis of the AF Lep light curve from the Transiting Exoplanet Survey Satellite (TESS) are described in Section 3. In Section 4, the relative astrometry of AF Lep b is used to confirm common proper motion with its host star and carry out an orbit fit. We also compare the orbital inclination with the stellar inclination to assess consistency with spin–orbit alignment. A summary of our results can be found in Section 5.

2. AF Lep: A Young Sun-like Star

AF Leporis (=AF Lep, HD 35850, HIP 25486, HR 1817) is a bright ($V = 6.30 \pm 0.01$ mag; Høg et al. 2000) F8V star (Gray et al. 2006) in the β Pic moving group (Zuckerman & Song 2004). It has a distance of 26.84 pc (Gaia Collaboration et al. 2021), an age of 24 ± 3 Myr (Bell et al. 2015), and a mass of $1.20 \pm 0.06\,M_\odot$ (Kervella et al. 2022). The properties of AF Lep are summarized in Table 1. An infrared excess based on WISE, Spitzer/MIPS, and Herschel/PACS photometry indicates that AF Lep has a debris disk, and spectral energy distribution (SED) modeling implies the disk radius is located at 46 ± 9 au although its unresolved nature means it could conceivably lie anywhere from 30 to 70 au (Pawellek et al. 2021; Pearce et al. 2022). Using dynamical arguments, Pearce et al. (2022) inferred that a single planet with a minimum mass of $1.1 \pm 0.2\,M_{\rm Jup}$ at a maximum semimajor axis of 35 ± 6 au would truncate the disk's inner edge. The minimum planetary mass increases steeply as its semimajor axis decreases, so a more massive planet closer in could also interact with the disk in a similar fashion. In a multi-planet scenario, the required planet mass is much lower ($0.09 \pm 0.03\,M_{\rm Jup}$). AF Lep has been frequently targeted in direct-imaging exoplanet searches (Biller et al. 2013; Stone et al. 2018; Nielsen et al. 2019; Launhardt et al. 2020). These searches did not find any close companions.

AF Lep is listed as an SB2 in the chromospherically active binary catalog complied by Eker et al. (2008). The initial double-lined spectroscopic binary classification was reported in Nordström et al. (2004), who found broad-line profiles with structure and variable central positions (B. Nordström 2022, private communication). This variability may be caused by a close binary but could also originate from strong imprints from starspot-related activity. Indeed, Zúñiga-Fernández et al. (2021) did not identify AF Lep as a single- or double-lined spectroscopic binary based on their recent high-resolution optical spectroscopy of this system. Additional spectroscopic monitoring would help clarify the binary nature of the host star. Because the original classification of AF Lep as an SB2 has not been validated with follow-up observations, for this work we treat AF Lep as a single active young star.

AF Lep exhibits a significant[15] astrometric acceleration between Hipparcos and Gaia DR3 in the HGCA. The HGCA provides three proper motion measurements: the proper motions at the Hipparcos and Gaia epochs and a joint average proper motion from the difference in sky position between the two missions. The average[16] tangential acceleration between the Gaia proper motion and the joint proper motion is 0.0191 ± 0.0024 mas yr^{-2}, which corresponds to a physical acceleration of 2.43 ± 0.30 m s^{-1} yr^{-1} at the distance of AF Lep. The predicted mass of a companion causing this acceleration would fall in the planetary regime if located within ≈30 au (see Figure 1).

---

[14] AF Lep b was also independently and contemporaneously discovered by De Rosa et al. (2023) and Mesa et al. (2023), both using Very Large Telescope/SPHERE.

[15] $\chi^2 = 77$, which corresponds to 8.5σ for 2 degrees of freedom.

[16] The average acceleration is computed across a baseline of 12.6 yr. Note, though, that the joint proper motion reflects the motion of AF Lep over the entire 25 yr between the two missions.

3. Observations

3.1. Keck/NIRC2 Adaptive Optics Imaging

We obtained high-contrast imaging of AF Lep on UT 2021 December 21 and UT 2023 February 3 with the NIRC2 camera at W.M. Keck Observatory. Our observations were carried out in L'-band (3.426–4.126 μm) with the VVC (Serabyn et al. 2017) and natural guide star adaptive optics (Wizinowich 2013) with the Shack–Hartmann wavefront sensor. Imaging was taken in groups of 25 frames using the quadrant analysis of coronagraphic images for tip-tilt sensing (`QACITS`; Huby et al. 2015, 2017) algorithm to center the host star behind the VVC. Each subsequence includes an off-axis unsaturated image of the host star for flux calibration and sky background frames for both the science images and the flux calibration frame. The science exposures have integration times of 0.18 s with 120 coadds. We used a subarray of 512 × 512 pixels for shorter readout times. For the 2021 December epoch, our total integration time was 39.6 minutes, amounting to $35\overset{\circ}{.}8$ of frame rotation. For the 2023 February epoch, our total integration time was 131.4 minutes, yielding $85\overset{\circ}{.}5$ of frame rotation. The Differential Image Motion Monitor (DIMM) seeing during our 2021 December observations averaged $0\overset{''}{.}5$; the average DIMM seeing during our 2023 February epoch was $0\overset{''}{.}6$.

Our data reduction for both data sets begins with subtracting darks and flat-fielding. The `L.A.Cosmic` algorithm (van Dokkum 2001) is then applied to identify and remove cosmic rays and hot pixels. We apply the distortion solution from Service et al. (2016) to correct for geometric distortions in the optics of the imaging system. The sky background is modeled and subtracted from both the science and off-axis flux calibration frames using principal component analysis (PCA) with the Vortex Image Processing (`VIP`; Gomez Gonzalez et al. 2017) package. Frames are co-registered to the sub-pixel level through a cross-correlation approach described in Guizar-Sicairos et al. (2008) and implemented in `scikit-image` (van der Walt et al. 2014) and `VIP`. Absolute centering is performed by fitting a negative Gaussian to the vortex core.

For carrying out PSF subtraction, we experimented with reductions from both `pyKLIP` (Wang et al. 2015) and `VIP`. Both packages use PCA (Amara & Quanz 2012; Soummer et al. 2012) to model and subtract the host-star PSF. For the 2021 December data set, the highest signal-to-noise ratio (S/N) is produced by a `pyKLIP` reduction with 20 annuli, 20 KL modes, and a value of one for the movement parameter. For the 2023 February imaging, the highest S/N is produced by a `VIP` reduction with 25 principal components. For the reduction of the 2023 February data set, the PSF is subtracted in annuli, with frames only included in the reference PSFs for a given science frame if they have more than 1 FWHM of parallactic angle rotation for the annulus. For each sequence, we then compute S/N maps by measuring the flux in 0.5-FWHM-radius circular apertures. The noise level is estimated through the flux measured in nonoverlapping circular apertures at the same separation. Figure 1 shows the S/N maps for our two epochs. We detect AF Lep b at a S/N of 7.5σ in the 2021 December imaging and 13.0σ in the 2023 February imaging.

To mitigate the introduction of systematics from the PSF-subtraction algorithm, we use the negative companion injection approach (e.g., Marois et al. 2008) to measure astrometry. A PSF template is generated by median-combining the off-axis flux calibration frames taken over each sequence. The inverse of this is then injected in the preprocessed frames at the approximate position, separation, and contrast of the companion, and the PSF-subtraction routine is performed. If the astrometry and photometry is well matched to the companion, its signal will be removed in the post-processed images. Otherwise, the companion's parameters are adjusted, the negative template is re-injected, and the PSF-subtraction routine is run again.

The injected astrometry and photometry are first coarsely optimized using the `AMOEBA` downhill simplex algorithm (Nelder & Mead 1965). We then use the `emcee` affine-invariant Markov Chain Monte Carlo (MCMC) ensemble sampler (Foreman-Mackey et al. 2013) with 100 walkers and 2×10^4 total steps to explore the astrometry and photometry parameter space. The sum of the residuals within a 4 FWHM-radius circular aperture of the source is used within the MCMC sampler to assess the match of the injected PSF to the companion. The first 30% of each chain is discarded as burn-in. We evaluate convergence through both visual inspection of the chains and by verifying that subsections of the chains yield consistent astrometry. For the 2021 December data set, the companion only appears at a high S/N in the PCA reductions when a parallactic angle cut is applied in constructing the reference PSFs for a given science image. We use 85 PCs for measuring the astrometry of the 2021 December epoch, which produces the highest S/N among the PCA reductions. For the 2023 February imaging, the companion appears at a high S/N in reductions without a parallactic angle cut, so we do not include this cut in the astrometry measurement to increase computational efficiency. When a parallactic angle cut is not performed, the maximum S/N is produced by 16 PCs, so we adopt this for the measurement. Ultimately, the number of PCs and PSF-subtraction approach for the astrometry measurement and reduced images are each a balance between S/N, computational efficiency, and consistency in the approach for the two data sets.

The MCMC chains consist of separation ρ, position angle θ, and a flux scaling factor for the PSF template. Following Franson et al. (2022), we combine the uncertainties on the astrometry from the MCMC run with the uncertainties in the distortion solution, north alignment, and plate scale. We also incorporate a 4.5 mas centering uncertainty to account for the average performance of the `QACITS` algorithm (Huby et al. 2017). Our final astrometry for the 2021 December epoch is $\rho = 338 \pm 11$ mas and $\theta = 62\overset{\circ}{.}8 \pm 1\overset{\circ}{.}3$. Our astrometry for the 2023 February epoch is $\rho = 342 \pm 8$ mas and $\theta = 72\overset{\circ}{.}0 \pm 1\overset{\circ}{.}0$. Converting the flux scaling factor to contrast yields $\Delta L' = 10.11 \pm 0.25$ mag for the 2021 December epoch and $\Delta L' = 9.94 \pm 0.14$ mag for the 2023 February epoch. Incorporating the $W1$ magnitude of AF Lep[17] (4.92 ± 0.07 mag; Cutri et al. 2012), these correspond to apparent magnitudes of $L' = 15.03 \pm 0.26$ mag and $L' = 14.87 \pm 0.15$ mag, respectively, and absolute magnitudes of $M_{L'} = 12.89 \pm 0.26$ mag (2021 December) and $M_{L'} = 12.72 \pm 0.15$ mag (2023 February).

3.2. TESS Light Curve

AF Lep was observed with TESS (Ricker et al. 2015) in Sectors 5, 6, and 32, and processed following the procedure described in Bowler et al. (2023). The Science Processing Operations Center's Pre-search Data Conditioning Simple Aperture Photometry (PDCSAP; Jenkins et al. 2016) light curve was downloaded using the `lightkurve` package (Lightkurve Collaboration et al. 2018). Outlier photometric points are removed by flattening the light curve with a high-pass Savitzky–Golay filter and identifying all data outside of three standard deviations.

---

[17] Here we assume that $L' - W1 = 0$ since these filters are in the Rayleigh–Jeans tail of the F8 host star's SED.

Clear modulations are evident in the final light curve with an amplitude of 1%–2%. The rotation period and uncertainty measurements are calculated by producing a generalized Lomb–Scargle periodogram (Zechmeister & Kürster 2009), fitting a Gaussian to the highest periodogram peak, and adopting the resulting mean and standard deviation. This yields a raw periodicity of 1.007 ± 0.007 days. However, starspots on AF Lep could be located at mid-latitudes rather than the equator. If differential rotation is present, then this will impact the interpretation of these modulations as a rotation period. To account for this, we follow Bowler et al. (2023) by inflating the uncertainty assuming a solar-like absolute shear of 0.07 rad day^{-1}. Adding this uncertainty from potential differential rotation in quadrature with the uncertainty from the periodogram analysis gives a final adopted value for the rotation period of 1.007 ± 0.009 days. This is similar to values of 0.966 ± 0.002 days from Messina et al. (2017), 1.03 ± 0.03 days from Gaia Collaboration et al. (2022), and 1.01 ± 0.05 day from Zúñiga-Fernández et al. (2021).[18]

4. Results

4.1. Common Proper Motion

Our second epoch of relative astrometry from 2023 February shows no significant change in separation compared to the first epoch taken 13 months earlier (338 ± 11 mas compared to 342 ± 8 mas in 2023), but a large counterclockwise change in P.A. ($62.^{\circ}8 \pm 1.^{\circ}3$ compared to $72.^{\circ}0 \pm 1.^{\circ}0$ in 2023). To test whether this is consistent with a stationary background source, perfect co-movement with the host star, or co-movement plus orbital motion, we compare our measurements with the predicted trajectories in Figure 2 using the host-star sky coordinates, parallax, and proper motion. At epoch 2023.090, the predicted separation for a stationary source is 367 ± 10 mas, and the predicted P.A. is $56.^{\circ}4 \pm 1.^{\circ}0$. Although the second epoch separation is similar, our measured P.A. of AF Lep b differs by about $9.^{\circ}2$ between the two observations. This corresponds to a 2.0σ discrepancy in separation and an 11.0σ discrepancy in P.A. We thus find that the common proper motion test strongly favors the source being a gravitationally bound companion rather than a background star. The apparent motion between the two epochs is therefore a result of orbital motion, not seen in separation (0.3σ) but detected at the 5.6σ level in P.A. Assuming linear motion, the P.A. of AF Lep b is increasing by about 8° yr^{-1}.

4.2. Color–Magnitude Diagram and Inferred Mass

We generate a $M_{L'}$–$(H - L')$ color–magnitude diagram (CMD) of nearby substellar sources to compare against the L' photometry of AF Lep b using The UltracoolSheet (Best et al. 2020). Single objects in the compilation with $W1$-band magnitudes, parallaxes, and H-band magnitudes in the Maunakea Observatories (MKO) filter system (Tokunaga & Vacca 2005) are selected. We convert the $W1$-band magnitudes to L'-band magnitudes using the M_{W1}–L' relation derived in Franson et al. (2023). For the absolute L' magnitude of AF Lep b, we adopt the value from our 2023 February imaging of $M_{L'} = 12.72 \pm 0.15$ mag. Our CMD is shown in the lower panel of Figure 2. The photometry of AF Lep b would imply an early T-dwarf spectral type although at the young age and low gravity of the companion, thick clouds may significantly redden the spectrum (e.g., Liu et al. 2016a; Faherty et al. 2016).

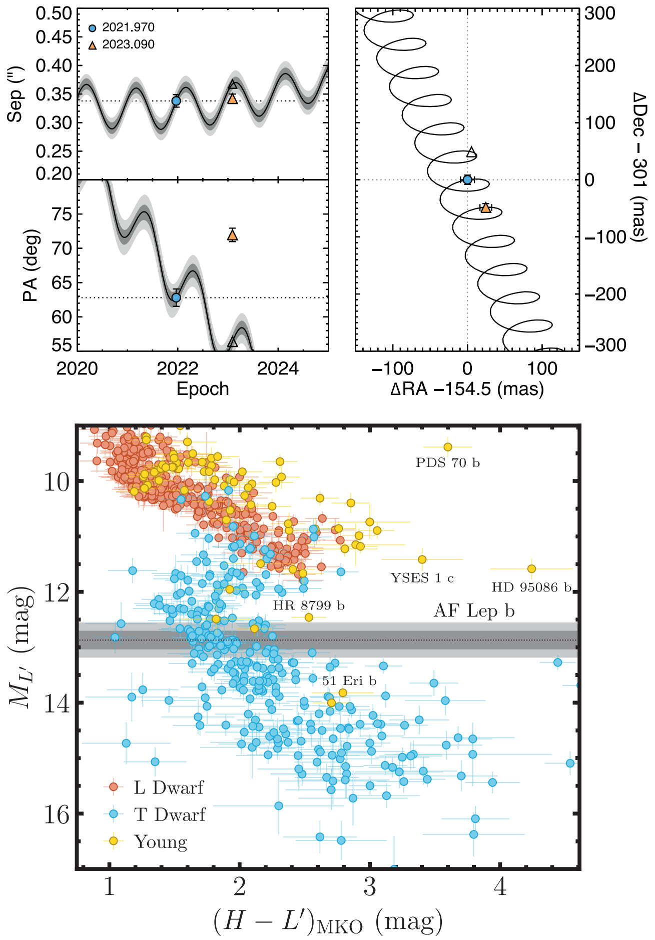

Figure 2. Top: test for common proper motion based on the two epochs of relative astrometry between AF Lep A and b. The left panels show the predicted relative motion of a stationary source in separation (top) and P.A. (bottom) with respect to the first epoch of relative astrometry (blue circles). Gray shaded regions represent 1σ and 2σ uncertainties. The predicted position at 2023.090 is plotted as an open triangle, and the orange triangles are our measurements. Our 2023 observations significantly disagree with a stationary background source model at the 11σ-level in P.A. The right panel shows the same comparison but in ΔR.A. and Δdecl. instead of separation and P.A. Bottom: comparison of our L' photometry of AF Lep b to the $M_{L'}$–$(H - L')$ CMD. The gray regions show the 1σ and 2σ uncertainties on the L' magnitude from our 2023 imaging. The background points show L (red) and T (blue) dwarfs from The UltracoolSheet (Best et al. 2020). Sources marked as young or low surface gravity are plotted in yellow. Young objects in the compilation are sources with independent age constraints <300 Myr. Low surface gravity sources have spectroscopic features of youth based on near-infrared spectroscopy. We also add substellar companions with H and L' photometry compiled within the `species` package (Stolker et al. 2020). The L' photometry of AF Lep b implies an early T-dwarf spectral type.

---

[18] Note that the Zúñiga-Fernández et al. (2021) measurement only used Sector 5 of the TESS light curve of AF Lep, which may contribute to its higher uncertainty.

From our absolute L' photometry, we can determine the model-inferred mass of AF Lep b given its age of 24 ± 3 Myr. Our approach is to draw from the age and absolute L' magnitude distributions 10^6 times and interpolate a given hot-start model grid to determine the corresponding mass distribution. We perform this procedure for both Cond (Baraffe et al. 2003) and the `ATMO-2020` (Phillips et al. 2020) models. This yields hot-start model-inferred masses of $4.53^{+0.32}_{-0.35}\,M_{\rm Jup}$ for Cond and $5.4 \pm 0.5\,M_{\rm Jup}$ for `ATMO-2020`. We can also infer masses from the Burrows et al. (1997) and Saumon & Marley (2008) grids by determining the bolometric luminosity of AF Lep b and interpolating the models. We base our bolometric correction on HR 8799 b, which has a similar L' absolute magnitude to AF Lep b ($M_{L'} = 12.66 \pm 0.11$ mag; Marois et al. 2010). Following the procedure outlined in Brandt et al. (2021a), the bolometric luminosity of HR 8799 b is $\log(L/L_{\rm bol}) = -4.79 \pm 0.10$ dex, which corresponds to a bolometric correction $BC(L') = -0.68 \pm 0.27$ mag. Applying this correction, the bolometric luminosity of AF Lep b is then $\log(L/L_{\rm bol}) = -4.81 \pm 0.13$ dex. This produces inferred masses of $6.2^{+1.0}_{-0.9}\,M_{\rm Jup}$ for Burrows et al. (1997) and $5.6^{+0.7}_{-0.7}\,M_{\rm Jup}$ for the Saumon & Marley (2008) grid with the hybrid prescription for clouds. The cloud-free and cloudy versions of the Saumon & Marley (2008) models yield masses of $6.1^{+0.9}_{-0.8}\,M_{\rm Jup}$ and $6.3^{+1.0}_{-0.9}\,M_{\rm Jup}$, respectively.

4.3. Orbit Fit and Dynamical Mass

Here, we perform a joint orbit fit with `orvara` (Brandt et al. 2021b) of our Keck/NIRC2 relative astrometry, archival RVs, and the HGCA proper motions. The archival RVs were published in Butler et al. (2017) and consist of 20 measurements with the HIRES spectrograph (Vogt et al. 1994) on Keck I. The observations were taken from 2002 September to 2013 November and have a median reported uncertainty of $63.2\ {\rm m\ s^{-1}}$ and an rms of $188.7\ {\rm m\ s^{-1}}$.

`orvara` uses the parallel-tempered MCMC ensemble sampler in `emcee` to infer the orbit element posteriors. The following orbital elements are directly fit: companion mass $M_{\rm comp}$, primary mass $M_{\rm host}$, semimajor axis a, inclination i_o, longitude of ascending node Ω, longitude at the reference epoch of 2010.0 $\lambda_{\rm ref}$, and RV jitter $\sigma_{\rm RV}$. Eccentricity e and argument of periastron ω are parameterized as $\sqrt{e}\,\sin\omega$ and $\sqrt{e}\,\cos\omega$ to avoid the Lucy–Sweeney bias against circular orbits (Lucy & Sweeney 1971). `orvara` analytically marginalizes over parallax, barycentric proper motion μ_α and μ_δ, and RV instrumental zero-points. We adopt uniformative priors for all quantities except host-star mass, where we take a prior of $1.2 \pm 0.06\ {\rm M}_\odot$ from its mass in Kervella et al. (2022). We use 20 temperatures, 100 walkers, and 5×10^5 total steps (5000 steps per walker) in the orbit fit. The first 20% of each chain is discarded as burn-in. Convergence is assessed by verifying that multiple runs with different starting parameters produce consistent parameter posteriors.

Table 2 shows the results of our orbit fit. Figure 3 displays the posterior distributions for selected orbit elements alongside a comparison of the relative astrometry of AF Lep b to a swarm of orbits drawn from the fit. We measure a dynamical mass of $3.2^{+0.7}_{-0.6}\,M_{\rm Jup}$, semimajor axis of $8.4^{+1.1}_{-1.3}$ au, orbital inclination of $50^{+9}_{-12}\,^\circ$, and eccentricity of $0.24^{+0.27}_{-0.15}$. The orbital period is 22 ± 5 yr, and the time of periastron is $T_0 = 2014.1^{+2.1}_{-3.2}$. AF Lep b and its host star have a mass ratio of 0.0026 ± 0.0005.

Table 1
Properties of AF Lep A and b

Property	Value	References
	AF Lep A	
$\alpha_{2000.0}$	05:27:04.76	1
$\delta_{2000.0}$	−11:54:03.5	1
μ_α[a] (mas yr^{-1})	16.915 ± 0.018	1
μ_δ (mas yr^{-1})	-49.318 ± 0.016	1
a[b] (mas yr^{-2})	0.0191 ± 0.0024	3
a[b] (m s^{-1}yr^{-1})	2.43 ± 0.30	3
π (mas)	37.254 ± 0.020	1
Distance (pc)	26.843 ± 0.014	1
SpT	F8V	2
Mass ($M_\odot$)	1.20 ± 0.06	3
Radius ($R_\odot$)	1.25 ± 0.06	4
Age (Myr)	24 ± 3	5
$T_{\rm eff}$ (K)	6130 ± 60	6
[Fe/H] (dex)	$+0.19 \pm 0.02$	7
$v \sin i$ (km/s)	50 ± 5	8
$\log(R'_{\rm HK})$ (dex)	−4.27	9
$\log(L_X/L_{\rm bol})$ (dex)	−3.48	10
$P_{\rm rot}$ (d)	1.007 ± 0.009	11
i_* (°)	54^{+11}_{-9}	11
RUWE$_{\rm DR3}$	0.918	1
B (mag)	6.83 ± 0.02	12
V (mag)	6.30 ± 0.01	12
Gaia G (mag)	6.210 ± 0.003	1
J (mag)	5.27 ± 0.03	13
H (mag)	5.09 ± 0.03	13
K_s (mag)	4.93 ± 0.02	13
$W1$ (mag)	4.92 ± 0.07	14
	AF Lep b	
$\rho_{2021.970}$ (mas)	338 ± 11	11
$\theta_{2021.970}$ (°)	62.8 ± 1.3	11
$\rho_{2023.090}$ (mas)	342 ± 8	11
$\theta_{2023.090}$ (°)	72.0 ± 1.0	11
$\Delta L'$ (mag)	9.94 ± 0.14	11
L' (mag)	14.87 ± 0.15	11
$M_{L'}$ (mag)	12.72 ± 0.15	11
$\log(L/L_{\rm bol})$ (dex)	-4.81 ± 0.13	11
Dynamical Mass ($M_{\rm Jup}$)	$3.2^{+0.7}_{-0.6}$	11
Semimajor Axis (au)	$8.4^{+1.1}_{-1.3}$	11
e	$0.24^{+0.27}_{-0.14}$	11
i_o (°)	50^{+9}_{-12}	11
Period (yr)	22 ± 5	11

References. (1) Gaia Collaboration (2022), (2) Gray et al. (2006), (3) Kervella et al. (2022), (4) Kervella et al. (2004), (5) Bell et al. (2015), (6) Ammons et al. (2006), (7) Gáspár et al. (2016), (8) Glebocki & Gnacinski (2005), (9) Isaacson & Fischer (2010), (10) Wright et al. (2011), (11) this work, (12) Høg et al. (2000), (13) Skrutskie et al. (2006), (14) Cutri et al. (2012).

[a] Proper motion in R.A. includes a factor of $\cos\delta$.

[b] Calculated from the proper motion difference between the Hipparcos-Gaia joint proper motion and the Gaia EDR3 proper motion in Brandt (2021).

To assess the potential of systematics in the relative astrometry or Hipparcos-Gaia proper motions impacting the companion's dynamical mass, we perform a suite of additional orbit fits to synthetic data with systematic offsets from the nominal measurements at the 2σ and 4σ levels. Each of these fits uses 20 temperatures, 100 walkers, and 10^5 steps. We first vary each epoch of the relative astrometry by $\pm 2\sigma$ and $\pm 4\sigma$ while keeping the other epoch constant. Here, the separation

Table 2
AF Lep b Orbit Fit Results

Parameter	Median $\pm 1\sigma$	95.4% C.I.	Prior
Fitted Parameters			
$M_{\rm comp}$ ($M_{\rm Jup}$)	$3.2^{+0.7}_{-0.6}$	(2.1, 4.7)	$1/M_{\rm comp}$ (log-flat), $M_{\rm comp} \in (0,\ 10^3\ M_\odot]$[c]
$M_{\rm host}$ ($M_\odot$)	1.20 ± 0.06	(1.08, 1.32)	$1.20 \pm 0.06\ M_\odot$ (Gaussian)
a (au)	$8.4^{+1.1}_{-1.3}$	(6.2, 12.8)	$1/a$ (log-flat), $a \in (0,\ 2 \times 10^5$ au][c]
i_o (°)	50^{+9}_{-12}	(23, 66)	$\sin(i)$, $0° < i < 180°$
$\sqrt{e}\,\sin\omega$	$-0.1^{+0.5}_{-0.4}$	(−0.8, 0.7)	Uniform, $-\sqrt{e} \leqslant \sqrt{e}\,\sin\omega \leqslant \sqrt{e}$
$\sqrt{e}\,\cos\omega$	$-0.16^{+0.40}_{-0.26}$	(−0.60, 0.58)	Uniform, $-\sqrt{e} \leqslant \sqrt{e}\,\cos\omega \leqslant \sqrt{e}$
Ω (°)	66^{+13}_{-22}[a]	(10, 122)[a]	Uniform, $-180° \leqslant \omega \leqslant 540°$
$\lambda_{\rm ref}$ (°)[b]	160^{+70}_{-90}	(10, 350)	Uniform, $-180° \leqslant \lambda_{\rm ref} \leqslant 540°$
Parallax (mas)	37.254 ± 0.020	(37.214, 37.293)	37.254 ± 0.020 mas (Gaussian)
μ_α (mas yr^{-1})	17.111 ± 0.024	(17.074, 17.154)	Uniform, $\mu_\alpha \in (-\infty\ ,\ \infty\ )$[c]
μ_δ (mas yr^{-1})	$-49.183^{+0.021}_{-0.017}$	(−49.211, −49.142)	Uniform, $\mu_\delta \in (-\infty\ ,\ \infty\ )$[c]
RV Jitter $\sigma_{\rm RV}$ (m s^{-1})	177^{+39}_{-30}	(124, 265)	$1/\sigma_{\rm RV}$ (log-flat), $\sigma_{\rm RV} \in (0,\ 10^3$ m s^{-1}][c]
Derived Parameters			
P (yr)	22 ± 5	(14, 42)	. . .
e	$0.24^{+0.27}_{-0.15}$	(0.02, 0.71)	. . .
ω (°)	210^{+80}_{-100}	(20, 340)	. . .
T_0 (JD)	2456700^{+800}_{-1200}	(2448400, 2458500)	. . .
T_0 (yr)	$2014.1^{+2.1}_{-3.2}$	(1991.3, 2019.1)	. . .
q ($=M_{\rm comp}/M_{\rm host}$)	0.0026 ± 0.0005	(0.0017, 0.0037)	. . .

Notes.

[a] The posterior distribution for Ω consists of two distinct peaks separated by 180°. The values shown in the table correspond to the lower peak. The other peak is located at 250^{+60}_{-40}° with a 95.4% confidence interval of (170, 350).

[b] Mean longitude at the reference epoch of 2010.0.

[c] Note that these are improper priors since they do not normalize to one.

and position angle are both offset by the same amount for each instance (for example, $+4\sigma$ in separation and $+4\sigma$ in position angle). We find that the dynamical mass is resilient to systematics at the 2σ and 4σ levels for both epochs, with all resultant companion masses being consistent with our dynamical mass to within 1σ. The companion mass posteriors from the mock runs have similar uncertainties to the dynamical mass. Changes to the HGCA proper motions have a larger impact on the dynamical mass. Shifting the Hipparcos-Gaia proper motion by -2σ or the Gaia proper motion by $+2\sigma$ decreases the dynamical mass by about 1σ from our nominal case to $\approx 2.5\ M_{\rm Jup}$. Applying the opposite offset increases the dynamical mass by about 1σ to $\approx 3.9\ M_{\rm Jup}$. Offsets at the 4σ level change the dynamical mass by about 2σ to about $1.7\ M_{\rm Jup}$ or $4.5 M_{\rm Jup}$. We thus find that the dynamical mass is more significantly affected by systematics in the Hipparcos-Gaia proper motions than the relative astrometry.

Our dynamical mass measurement is slightly lower than model-inferred masses from the planet's L' photometry and associated bolometric luminosity. It is 1.7σ lower than the Cond-inferred mass of $4.53^{+0.32}_{-0.35}\ M_{\rm Jup}$, 2.6σ lower than the mass inferred via `ATMO-2020` of $5.4 \pm 0.5\ M_{\rm Jup}$, 2.7σ lower than the mass inferred from Burrows et al. (1997) of $6.2^{+1.0}_{-0.9}\ M_{\rm Jup}$, and 2.4σ lower than the Saumon & Marley (2008)-inferred mass with the hybrid prescription for clouds. Here, one-sided Gaussian-equivalent σ values are determined following Franson et al. (2023). All inferred masses are generated using hot-start models, which treat planets as having arbitrarily large radii and high entropies at early ages as an initial condition. Cold- (e.g., Marley et al. 2007; Fortney et al. 2008) and warm-start (e.g., Spiegel & Burrows 2012; Marleau & Cumming 2014) models start with lower amounts of initial entropy to emulate the loss of energy through accretion shocks in planet formation. Since this lowers the luminosity of planets at young ages relative to hot-start models, the discrepancy between our dynamical mass and model predictions is *larger* if a cold- or warm-start model is assumed.

One way this modest discrepancy can be reconciled is if the planet is younger than the star, perhaps due to delayed formation in a disk. This would cause the planet to be brighter than expected based on the host-star age. For the case of AF Lep b, the planet would require an age of 16^{+7}_{-5} Myr for the Cond mass to match the dynamical mass. Other models require lower masses; for the prediction from the hybrid Saumon & Marley (2008) model to match the dynamical mass, the planet would need to be 9^{+4}_{-3} Myr. This would imply a formation timescale of ≈5–15 Myr, which would suggest formation via core accretion, which takes many Myr to operate, over rapid giant planet formation via disk instability. Typical protoplanetary disk lifetimes are 5–10 Myr for Sun-like and lower-mass ($<2\ M_\odot$) stars (Pfalzner et al. 2022). Other possibilities for resolving this discrepancy include a younger age of the system, young L/T transition objects being more luminous than predicted by current evolutionary models, and another planet in the system biasing the dynamical mass measurement.

4.4. *Planet–Disk Interactions*

There are several potential avenues for an inner planet to dynamically interact with an outer debris disk. One possibility is the planet truncating the disk's inner edge. Due to the close separation of AF Lep b from its host star, it is unlikely that the

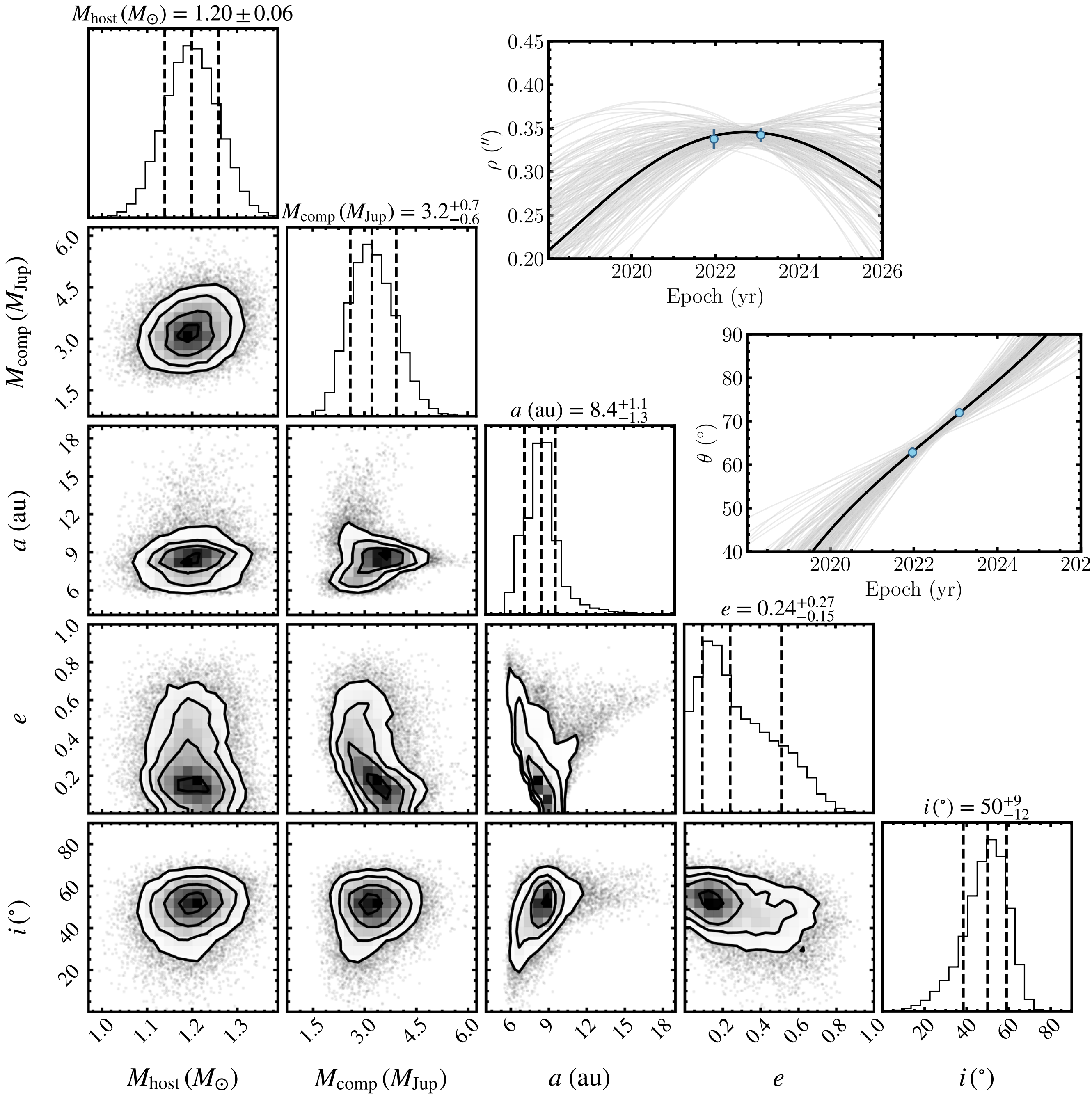

Figure 3. Joint posterior distributions of $M_{\rm host}$, $M_{\rm comp}$, a, e, and i for the orbit fit of AF Lep b. The diagonal panels show the marginalized distribution for each parameter. The contours on off-diagonal panels denote 1σ, 2σ, 3σ, and 4σ levels in the joint posteriors. The upper right plots compare the separation and position angle of AF Lep b over time against a swarm of orbits drawn from the orbit fit, shown in gray. The black curves highlight the maximum-likelihood orbit.

planet is truncating the disk from its current orbit. Pearce et al. (2022) found that the disk inner edge could be truncated by a $1.1 \pm 0.2\,M_{\rm Jup}$ planet at a semimajor axis of 35 ± 6 au. Larger objects at closer-in semimajor axes could also produce the same effect, but the dependence between mass and semimajor axis is sufficiently steep that by the 8 au semimajor axis of AF Lep b, only stellar companions are capable of truncating the disk (see Equation (6) of Pearce et al. 2022). This remains the case if we allow for the possible eccentricity of AF Lep b and the uncertain location of the unresolved disk. If the debris disk was truncated by planets, then either additional, unseen planets are responsible or AF Lep b was closer to the disk in the past and has since migrated inwards.

While AF Lep b is unlikely to be truncating the disk, its possible eccentricity could drive the disk into an asymmetric shape. Equation (5) in Pearce et al. 2022 relates the semimajor axis and eccentricity of a planet's orbit to the eccentricities of a debris disk's edges. A planet at 8 au with an eccentricity of 0.25 would drive a narrow disk at 46 au to an eccentricity of ∼0.1. The disk is currently unresolved, so no eccentricity or width information is available. Future resolved observations of the disk have the potential to determine the disk's eccentricity and directly examine the interaction between an eccentric planet and its debris disk.

A third possibility is stirring, where the planet excites planetesimals in the disk, causing them to collide and release the observed dust. Equation (15) of Mustill & Wyatt (2009) gives the mass of an interior planet required to stir debris as a function of planet eccentricity and location. For an eccentricity of 0.25 and semimajor axis of 8 au, planets with masses greater than 0.45 M_{Jup} are able to stir the AF Lep debris disk. AF Lep b, with its mass of $3.2^{+0.7}_{-0.6}\,M_{\mathrm{Jup}}$, may be actively stirring the disk. This is significant as there is growing evidence that many debris disks are unable to stir themselves via self-gravity (Krivov & Booth 2018; Pearce et al. 2022, though see also Najita et al. 2022). Planetary stirring could therefore be prevalent in generating the observed dust in debris disks. Note that if AF Lep b has a small but nonzero eccentricity, it could still stir the disk, provided the eccentricity is above ≈0.04. This threshold is determined by rearranging Equation (15) of Mustill & Wyatt (2009) to give the minimum eccentricity capable of stirring the disk as a function of planet mass.

4.5. Stellar Inclination and Minimum Obliquity

The line-of-sight inclination of AF Lep, i_*, can be inferred from its rotation period, stellar radius, and projected rotational velocity. We follow the Bayesian framework of Masuda & Winn (2020) to derive i_* using the analytical expression for its posterior distribution from Bowler et al. (2023, their Equation (9)), which accounts for the correlation between projected and equatorial rotational velocities. Here we adopt the TESS rotation period of 1.007 ± 0.009 d, the $v \sin i_*$ value of 50 ± 5 km s^{-1} from Glebocki & Gnacinski (2005), and radius of 1.25 ± 0.06 $R_\odot$ from Kervella et al. (2004). The maximum a posteriori value is 54°. The 68% credible interval spans 45°–65° and the 95% credible interval spans 39°–82°.

The stellar inclination together with the inclination of the orbital plane of AF Lep b (i_o) provides information about the minimum stellar obliquity—whether the spin axis of AF Lep is aligned or misaligned with respect to the planet. Our orbit fit indicates an inclination of $i_o = 50^{+9}_{-12}{}^\circ$. This is in excellent agreement with the stellar inclination of $i_* = 54^{+11}_{-9}{}^\circ$. The polar position angle of AF Lep—which describes its absolute orientation in the sky plane—is not known and can therefore not be compared with the longitude of ascending node of the orbit to assess the true obliquity angle. However, the agreement of the inclination angles is nevertheless consistent with spin–orbit alignment, which reinforces trends seen in other systems with imaged planets but differs from the more diverse architectures of brown dwarf companions (Bowler et al. 2023). The debris disk around AF Lep has not been resolved; if future observations resolve the disk, its inclination could be compared with the stellar and orbital inclinations to further assess angular momentum alignment in the AF Lep system.

5. Summary

AF Lep b is a young giant planet directly imaged inside the debris disk of a Sun-like star in the 24 ± 3 Myr β Pic moving group. The system was identified as a promising target based on the low-amplitude (2.43 ± 0.30 m s^{-1} yr^{-1}) astrometric acceleration the planet induces on its host star. Our main conclusions are summarized below:

1. Our two epochs of NIRC2 observations in L' with the VVC separated by 13 months confidently show that AF Lep b is gravitationally bound and is undergoing orbital motion around its host star. We can rule out AF Lep b being a background star at the 11σ level, and orbital motion is detected at the 6σ level.
2. AF Lep b has a contrast of $\Delta L' = 9.94 \pm 0.14$ mag at $0\farcs34$ and an absolute magnitude of $M_{L'} = 12.72 \pm 0.15$ mag. Based on the age of the host star, and assuming the planet was formed at the same time, the implied planet mass from hot-start evolutionary models is ≈4–6 M_{Jup}.
3. Our orbit fit incorporating the relative astrometry, astrometric acceleration, and RVs yields a dynamical mass of $3.2^{+0.7}_{-0.6}\,M_{\mathrm{Jup}}$, a semimajor axis of $8.4^{+1.1}_{-1.3}$ au, and a modest eccentricity of $0.24^{+0.27}_{-0.15}$ for AF Lep b. The mass of AF Lep b is too low at an orbital distance of ≈8 au to truncate the outer debris disk, which is located at $\sim 46 \pm 9$ au (Pearce et al. 2022). Another massive planet or series of low-mass planets may be present at wider separations.
4. The dynamical mass ($3.2^{+0.7}_{-0.6}\,M_{\mathrm{Jup}}$) is somewhat lower than predicted masses ($\approx 4 - 6\,M_{\mathrm{Jup}}$) from hot-start models assuming a nominal age of 24 ± 3 Myr from the host star. This could be caused by a slightly younger age for the host star, delayed formation in a disk, systematic uncertainties in the evolutionary models, or another companion in the system.
5. The stellar inclination ($i_* = 54^{+11}_{-9}{}^\circ$) and orbital inclination ($i_o = 50^{+9}_{-12}{}^\circ$) are in good agreement, which is consistent with the system having spin–orbit alignment although polar position angle of the star is unknown, so this agreement represents a lower limit on the true obliquity.

AF Lep joins other young planet hosts with debris disks such as β Pic, HR 8799, HD 206893, and HD 95086, reinforcing indications of a higher frequency of long-period planets orbiting stars hosting debris disks (Meshkat et al. 2017). Within the β Pic moving group, the mass of AF Lep b is higher than 51 Eri b (≈2 M_{Jup}; Macintosh et al. 2015) and lower than β Pic b and c (8–9 M_{Jup}; Nowak et al. 2020), contributing to a growing sequence of giant planets with common ages. AF Lep b is the lowest-mass imaged planet with a dynamical mass. We expect it to become an excellent target for follow-up orbital and atmospheric characterization.

Acknowledgments

K.F. acknowledges support from the National Science Foundation Graduate Research Fellowship Program under Grant No. DGE 2137420. B.P.B. acknowledges support from the National Science Foundation grant AST-1909209, NASA Exoplanet Research Program grant 20-XRP20_2-0119, and the Alfred P. Sloan Foundation. Y.Z. acknowledges support from the Heising-Simons Foundation 51 Pegasi b Fellowship. T.D.P. is supported by Deutsche Forschungsgemeinschaft (DFG) grants KR 2164/14-2 and KR 2164/15-2. Q.H.T. and B.P.B. acknowledge the support from a NASA FINESST grant (80NSSC20K1554). T.D. acknowledges support from UKRI STFC AGP grant ST/W001209/1. This work was supported by a NASA Keck PI Data Award, administered by the NASA Exoplanet Science Institute. This research has made use of the VizieR catalog access tool, CDS, Strasbourg, France (DOI: 10.26093/cds/vizier). The original description of the VizieR service was published in 2000, A&AS 143, 23. This publication makes use of data products from the Wide-field Infrared Survey Explorer, which is a joint project of the University of California, Los Angeles, and the Jet Propulsion

Laboratory/California Institute of Technology, funded by the National Aeronautics and Space Administration. This work has benefited from The UltracoolSheet at http://bit.ly/UltracoolSheet, maintained by Will Best, Trent Dupuy, Michael Liu, Rob Siverd, and Zhoujian Zhang, and developed from compilations by Dupuy & Liu (2012), Dupuy & Kraus (2013), Liu et al. (2016b), Best et al. (2018), Best et al. (2021).

The authors wish to recognize and acknowledge the very significant cultural role and reverence that the summit of Maunakea has always had within the indigenous Hawaiian community. We are most fortunate to have the opportunity to conduct observations from this mountain.

Facility: Keck:II (NIRC2).

Software: `VIP` (Gomez Gonzalez et al. 2017), `pyKLIP` (Wang et al. 2015), `orvara` (Brandt et al. 2021b), `ccdproc` (Craig et al. 2017), `photutils` (Bradley et al. 2019), `astropy` (Astropy Collaboration et al. 2013, 2018), `pandas` (McKinney 2010), `matplotlib` (Hunter 2007), `numpy` (Harris et al. 2020), `scipy` (Virtanen et al. 2020), `emcee` (Foreman-Mackey et al. 2013), `corner` (Foreman-Mackey 2016), `lightkurve` (Lightkurve Collaboration et al. 2018), `scikit-image` (van der Walt et al. 2014).

ORCID iDs

Kyle Franson https://orcid.org/0000-0003-4557-414X
Brendan P. Bowler https://orcid.org/0000-0003-2649-2288
Yifan Zhou https://orcid.org/0000-0003-2969-6040
Tim D. Pearce https://orcid.org/0000-0001-5653-5635
Daniella C. Bardalez Gagliuffi https://orcid.org/0000-0001-8170-7072
Lauren I. Biddle https://orcid.org/0000-0003-2646-3727
Timothy D. Brandt https://orcid.org/0000-0003-2630-8073
Justin R. Crepp https://orcid.org/0000-0003-0800-0593
Trent J. Dupuy https://orcid.org/0000-0001-9823-1445
Jacqueline Faherty https://orcid.org/0000-0001-6251-0573
Rebecca Jensen-Clem https://orcid.org/0000-0003-0054-2953
Marvin Morgan https://orcid.org/0000-0003-4022-6234
Aniket Sanghi https://orcid.org/0000-0002-1838-4757
Christopher A. Theissen https://orcid.org/0000-0002-9807-5435
Quang H. Tran https://orcid.org/0000-0001-6532-6755
Trevor N. Wolf https://orcid.org/0000-0002-1406-8829

References

Amara, A., & Quanz, S. P. 2012, MNRAS, 427, 948
Ammons, S. M., Robinson, S. E., Strader, J., et al. 2006, ApJ, 638, 1004
Astropy Collaboration, Price-Whelan, A. M., Sipőcz, B. M., et al. 2018, AJ, 156, 123
Astropy Collaboration, Robitaille, T. P., Tollerud, E. J., et al. 2013, A&A, 558, A33
Baraffe, I., Chabrier, G., Barman, T. S., Allard, F., & Hauschildt, P. H. 2003, A&A, 402, 701
Bate, M. R. 2009, MNRAS, 392, 590
Bell, C. P. M., Mamajek, E. E., & Naylor, T. 2015, MNRAS, 454, 593
Best, W. M. J., Dupuy, T. J., Liu, M. C., Siverd, R. J., & Zhang, Z. 2020, The UltracoolSheet: Photometry, Astrometry, Spectroscopy, and Multiplicity for 3000+ Ultracool Dwarfs and Imaged Exoplanets, v1.0.0, Zenodo, doi:10.5281/ZENODO.4169084
Best, W. M. J., Liu, M. C., Magnier, E. A., & Dupuy, T. J. 2021, AJ, 161, 42
Best, W. M. J., Magnier, E. A., Liu, M. C., et al. 2018, ApJS, 234, 1
Biller, B. A., Liu, M. C., Wahhaj, Z., et al. 2013, ApJ, 777, 160
Boss, A. P. 1997, Sci, 276, 1836
Bowler, B. P., Blunt, S. C., & Nielsen, E. L. 2020, AJ, 159, 63
Bowler, B. P., Endl, M., Cochran, W. D., et al. 2021, ApJL, 913, L26
Bowler, B. P., Tran, Q. H., Zhang, Z., et al. 2023, AJ, 165, 164
Bradley, L., Sipőcz, B., Robitaille, T., et al. 2019, astropy/photutils: v0.7.2, Zenodo, doi:10.5281/zenodo.3568287
Brandt, G. M., Brandt, T. D., Dupuy, T. J., Michalik, D., & Marleau, G.-D. 2021a, ApJL, 915, L16
Brandt, T. D. 2021, ApJS, 254, 42
Brandt, T. D., Dupuy, T. J., Li, Y., et al. 2021b, AJ, 162, 186
Brandt, T. D., Dupuy, T. J., & Bowler, B. P. 2019, AJ, 158, 140
Burrows, A., Marley, M., Hubbard, W. B., et al. 1997, ApJ, 491, 856
Butler, R. P., Vogt, S. S., Laughlin, G., et al. 2017, AJ, 153, 208
Chauvin, G., Desidera, S., Lagrange, A.-M., et al. 2017, A&A, 605, L9
Cheetham, A., Ségransan, D., Peretti, S., et al. 2018, A&A, 614, A16
Craig, M., Crawford, S., Seifert, M., et al. 2017, astropy/ccdproc: v1.3.0.post1, Zenodo, doi:10.5281/zenodo.1069648
Crepp, J. R., Johnson, J. A., Howard, A. W., et al. 2014, ApJ, 781, 29
Currie, T., Brandt, G. M., Brandt, T. D., et al. 2023, Sci, 380, 198
Cutri, R. M., Wright, E. L., Conrow, T., et al. 2012, yCat, II/311
De Rosa, R. J., Esposito, T. M., Hirsch, L. A., et al. 2019, AJ, 158, 225
De Rosa, R. J., Nielsen, E. L., Wahhaj, Z., et al. 2023, A&A, 672, A94
Dupuy, T. J., & Kraus, A. L. 2013, Sci, 341, 1492
Dupuy, T. J., & Liu, M. C. 2012, ApJS, 201, 19
Eker, Z., Ak, N. F., Bilir, S., et al. 2008, MNRAS, 389, 1722
Faherty, J. K., Riedel, A. R., Cruz, K. L., et al. 2016, ApJS, 225, 1
Foreman-Mackey, D. 2016, JOSS, 1, 24
Foreman-Mackey, D., Hogg, D. W., Lang, D., & Goodman, J. 2013, PASP, 125, 306
Fortney, J. J., Marley, M. S., Saumon, D., & Lodders, K. 2008, ApJ, 683, 1104
Franson, K., Bowler, B. P., Bonavita, M., et al. 2023, AJ, 165, 39
Franson, K., Bowler, B. P., Brandt, T. D., et al. 2022, AJ, 163, 50
Fulton, B. J., Rosenthal, L. J., Hirsch, L. A., et al. 2021, ApJS, 255, 0
Gaia Collaboration, Brown, A. G. A., Vallenari, A., et al. 2021, A&A, 649, A1
Gaia Collaboration, Vallenari, A., Brown, A. G. A., & Prusti, T. 2022, arXiv:2208.00211
Gáspár, A., Rieke, G. H., & Ballering, N. 2016, ApJ, 826, 171
Glebocki, R., & Gnacinski, P. 2005, yCat, III/244
Gomez Gonzalez, C. A., Wertz, O., Absil, O., et al. 2017, AJ, 154, 7
Gray, R. O., Corbally, C. J., Garrison, R. F., et al. 2006, AJ, 132, 161
Guizar-Sicairos, M., Thurman, S. T., & Fienup, J. R. 2008, OptL, 33, 156
Harris, C. R., Millman, K. J., van der Walt, S. J., et al. 2020, Natur, 585, 357
Hinkley, S., Lacour, S., Marleau, G. D., et al. 2023, A&A, 671, L5
Høg, E., Fabricius, C., Makarov, V. V., et al. 2000, A&A, 355, L27
Huby, E., Baudoz, P., Mawet, D., & Absil, O. 2015, A&A, 584, A74
Huby, E., Bottom, M., Femenia, B., et al. 2017, A&A, 600, A46
Hunter, J. D. 2007, CSE, 9, 90
Isaacson, H., & Fischer, D. 2010, ApJ, 725, 875
Jenkins, J. M., Twicken, J. D., McCauliff, S., et al. 2016, Proc. SPIE, 9913, 99133E
Johansen, A., & Lambrechts, M. 2017, AREPS, 45, 359
Keppler, M., Benisty, M., Müller, A., et al. 2018, A&A, 617, A44
Kervella, P., Arenou, F., & Thévenin, F. 2022, A&A, 657, A7
Kervella, P., Thévenin, F., Folco, E. D., & Ségransan, D. 2004, A&A, 426, 297
Krivov, A. V., & Booth, M. 2018, MNRAS, 479, 3300
Lagrange, A.-M., Bonnefoy, M., Chauvin, G., et al. 2010, Sci, 329, 57
Launhardt, R., Henning, T., Quirrenbach, A., et al. 2020, A&A, 635, A162
Liu, M. C., Dupuy, T. J., & Allers, K. N. 2016a, ApJ, 833, 1
Liu, M. C., Dupuy, T. J., & Allers, K. N. 2016b, ApJ, 833, 96
Liu, M. C., Fischer, D. A., Graham, J. R., et al. 2002, ApJ, 571, 519
Lucy, L. B., & Sweeney, M. A. 1971, AJ, 76, 544
Lightkurve Collaboration, Cardoso, J. V. d. M, Hedges, C., et al. 2018, Astrophysics Source Code Library, ascl:1812.013
Macintosh, B., Graham, J. R., Barman, T., et al. 2015, Sci, 350, 64
Marleau, G.-D., & Cumming, A. 2014, MNRAS, 437, 1378
Marley, M. S., Fortney, J. J., Hubickyj, O., Bodenheimer, P., & Lissauer, J. J. 2007, ApJ, 655, 541
Marois, C., Macintosh, B., Barman, T., et al. 2008, Sci, 322, 1348
Marois, C., Zuckerman, B., Konopacky, Q. M., Macintosh, B., & Barman, T. 2010, Natur, 372, 1
Masuda, K., & Winn, J. N. 2020, AJ, 159, 81
McKinney, W. 2010, in Proc. 9th Python in Science Conf., ed. S. van der Walt & J. Millman (Austin, TX: SciPy), 56
Mesa, D., Gratton, R., Kervella, P., et al. 2023, A&A, 672, A93
Meshkat, T., Mawet, D., Bryan, M. L., et al. 2017, AJ, 154, 245
Messina, S., Lanzafame, A. C., Malo, L., et al. 2017, A&A, 607, A3
Mustill, A. J., & Wyatt, M. C. 2009, MNRAS, 399, 1403
Nagpal, V., Blunt, S., Bowler, B. P., et al. 2023, AJ, 165, 32
Najita, J. R., Kenyon, S. J., & Bromley, B. C. 2022, ApJ, 925, 45

Nelder, J. A., & Mead, R. 1965, CompJ, 7, 308
Nielsen, E. L., Rosa, R. J. D., Macintosh, B., et al. 2019, AJ, 158, 13
Nordström, B., Mayor, M., Andersen, J., et al. 2004, A&A, 418, 989
Nowak, M., Lacour, S., Lagrange, A.-M., et al. 2020, A&A, 642, L2
Pawellek, N., Wyatt, M., Matrà, L., Kennedy, G., & Yelverton, B. 2021, MNRAS, 502, 5390
Pearce, T. D., Launhardt, R., Ostermann, R., et al. 2022, A&A, 659, A135
Perets, H. B., & Kouwenhoven, M. B. N. 2012, ApJ, 750, 83
Pfalzner, S., Dehghani, S., & Michel, A. 2022, ApJL, 939, L10
Phillips, M. W., Tremblin, P., Baraffe, I., et al. 2020, A&A, 637, A38
Pollack, J. B., Hubickyj, O., Bodenheimer, P., et al. 1996, Icar, 124, 62
Rameau, J., Chauvin, G., Lagrange, A.-M., et al. 2013, ApJL, 772, L15
Ricker, G. R., Winn, J. N., Vanderspek, R., et al. 2015, JATIS, 1, 014003
Saumon, D., & Marley, M. S. 2008, ApJ, 689, 1327
Serabyn, E., Huby, E., Matthews, K., et al. 2017, AJ, 153, 43
Service, M., Lu, J. R., Campbell, R., et al. 2016, PASP, 128, 095004
Skrutskie, M. F., Cutri, R. M., Stiening, R., et al. 2006, AJ, 131, 1163
Soummer, R., Pueyo, L., & Larkin, J. 2012, ApJ, 755, L28
Spiegel, D. S., & Burrows, A. 2012, ApJ, 745, 174
Stolker, T., Quanz, S. P., Todorov, K. O., et al. 2020, A&A, 635, A182
Stone, J. M., Skemer, A. J., Hinz, P. M., et al. 2018, AJ, 156, 286
Tokunaga, A. T., & Vacca, W. D. 2005, PASP, 117, 421
van der Walt, S., Schönberger, J. L., Nunez-Iglesias, J., et al. 2014, PeerJ, 2, e453
van Dokkum, P. 2001, PASP, 113, 1420
Virtanen, P., Gommers, R., Oliphant, T. E., et al. 2020, NatMe, 17, 261
Vogt, S. S., Allen, S. L., Bigelow, B. C., et al. 1994, Proc. SPIE, 2198, 362
Wagner, K., Apai, D., & Kratter, K. M. 2019, ApJ, 877, 46
Wang, J. J., Ruffio, J.-B., De Rosa, R. J., et al. 2015, pyKLIP: PSF subtraction for exoplanets and disks, Astrophysics Source Code Library, ascl:1506.001
Wizinowich, P. 2013, PASP, 125, 798
Wright, N. J., Drake, J. J., Mamajek, E. E., & Henry, G. W. 2011, ApJ, 743 48
Zechmeister, M., & Kürster, M. 2009, A&A, 496, 577
Zuckerman, B., & Song, I. 2004, ARA&A, 42, 685
Zúñiga-Fernández, S., Bayo, A., Elliott, P., et al. 2021, A&A, 645, A30